JOURNAL OF GEOPHYSICAL RESEARCH, VOL. 103, NO. A12, PAGES 29,705–29,717, DECEMBER 1, 1998

Electron temperature in the solar wind: Generic radial variation from kinetic collisionless models

Nicole Meyer-Vernet and Karine Issautier

Département de Recherche Spatiale, CNRS, Observatoire de Paris, Meudon, France

Abstract. We calculate analytically the radial profile of the average electron temperature in the solar wind with a kinetic collisionless model. The electron temperature profile at large distances r is the sum of a term $\propto r^{-4/3}$ plus a constant, with both terms of the same order of magnitude near $r \sim 1$ AU. This result is generic as it is weakly dependent on the particle velocity distributions in the corona. It provides a natural explanation for the observed electron temperature profile near 1 AU, which is in the low or middle part of the range between isothermal and adiabatic behaviors. The $r^{-4/3}$ term comes from the isotropically distributed electrons confined by the heliospheric electric potential, which is found to have a similar radial variation. The constant term comes from the parallel temperature of the electrons energetic enough to escape. The calculated profile flattens as r increases and tends to be flatter in the high-speed wind. We also give simple explicit expressions for the electron temperature and density at large distances and for the terminal wind velocity as a function of coronal parameters when the electron velocity distribution is a Kappa function, which is close to a Maxwellian with a suprathermal tail.

1. Introduction

Since the transport of thermal energy by electrons is believed to play a key role in thermally driven solar wind models, the measured electron temperature radial profile is an important ingredient to constrain the theories. Evaluations of radial temperature gradients for electrons are generally made for simplicity as power law approximations of the form $T_e \propto 1/r^{\beta}$. There is a large scatter in the measurements, which give values generally in the low or middle part of the range $\beta = [0 - 4/3]$, whose limits correspond respectively to isothermal and adiabatic (isotropic) behavior [see *Schwenn and Marsch*, 1991, and references therein]. The profiles tend to be flatter in the high-speed wind and to flatten with increasing heliocentric distance in this type of wind [see *Pilipp et al.*, 1990]. There is, however, no overall agreement between the existing results, which is not surprising because it is difficult to separate genuine variations along stream flux tubes from variations across them and from nongeneric effects due to temporal variations or to the contingencies of the experimental setup.

What is the origin of the observed average electron temperature gradient? Can it be explained by first principles? An obvious theoretical difficulty is that the particle free paths are nowhere sufficiently small in the solar wind (including its base) [*Scudder and Olbert*, 1983] to justify a fluid description closed by using the classical Spitzer-Härm conductivity [*Spitzer and Härm*, 1953], nor sufficiently large to justify a collisionless kinetic description. However, the collisions between particles change their velocity directions and redistribute their energies, but they do not change significantly the mean electron kinetic energy owing to the large ion-to-electron mass ratio. In other words, although collisions do change the shape of the velocity distributions and, in particular, reduce the large thermal anisotropies given by exospheric models [*Jockers*, 1970; *Lemaire and Scherer*, 1971], they are not expected to change significantly the average electron temperature

$$T_e = m_e \left\langle v^2 \right\rangle / 3k_B$$

Here m_e and k_B are the electron mass and Boltzmann's constant, respectively, and the angle brackets denote an average over the electron velocity distribution.

Hence it may be worth using collisionless models to predict the average electron temperature. This is not true of the proton temperature, which is affected by collisions with alpha particles [see *Hernandez et al.*, 1987, and references therein] and possibly by wave-particle interactions [see, for example, *Tu*, 1988].

Numerical results with a full exospheric solar wind model were obtained by assuming (truncated) Maxwellian velocity distributions at the base of the wind [*Lemaire and Scherer*, 1971]. Following the pioneering work of *Scudder* [1992a, b], the role of non-Maxwellian distributions was studied numerically by *Maksimovic et al.* [1997a]. Analytical results were obtained for the proton temperature at large distances by *Lemaire and Scherer* [1972]. The aim of this paper is to perform a similar analytical calculation for the electrons and with arbitrary velocity distributions in the corona. We will find, indeed, that this class of models yields an electron

Paper number 98JA02853.
0148-0227/98/98JA-02853$09.00

temperature radial profile that follows a simple generic law far from the Sun, weakly dependent on the particle velocity distributions in the corona.

In section 2 we recall the basics of an exospheric solar wind model. In section 3 we give general expressions for the moments of the velocity distributions far from the Sun and deduce analytically a generic radial profile for the electron temperature and the ambipolar potential. In section 4 we apply the results to a Kappa electron velocity distribution, which includes the Maxwellian as a limiting case, and give explicit approximate expressions for the electron density and temperature at large distances and for the terminal wind velocity. In section 5 we discuss our results in the context of the fluid momentum and energy balance equations. A summary and final remarks are given in section 6. Except otherwise stated, we use SI units; in the approximate results the symbol "$\approx$" means "approximately equal," whereas "$\sim$" means a looser approximation, i.e., "of the same order of magnitude."

2. Basics of a Kinetic Collisionless Model

We recall in this section the basic points of a self-consistent, kinetic collisionless solar wind model, with the formulation developed by *Lemaire and Scherer* [1971, 1973] and deduce general expressions for the moments of the particle velocity distributions.

2.1. Basic Physics

A key hypothesis of these models is that above a given reference level, called the "exobase," the particles are assumed collisionless. This allows one to calculate the velocity distribution of a given particle species above the exobase as a function of the distribution at the exobase by using Liouville's theorem with conservation of energy and magnetic moment.

An important point is that in an inertial frame the potential energy of a charged particle near a massive body is the sum of the gravitational energy and of the electrostatic energy due to the ambipolar field required by the large difference in mass of the electrons and ions. Let us first consider the simple case of electrons and protons in static equilibrium with the same temperature. Since the electrons barely see the gravitational field owing to their small mass, an electrostatic field is required to equalize the forces acting on the electrons and ions; the corresponding electrostatic force acting on the protons is one half the gravitational force and directed in the opposite direction (the Pannekoek-Rosseland result).

In an expanding atmosphere, however, as first shown by *Lemaire and Scherer* [1969] and *Jockers* [1970], the electrostatic potential is much larger. Otherwise, the escaping flux of electrons, which is proportional to their thermal velocity at the exobase for a Maxwellian velocity distribution, would be roughly $\sqrt{m_p/m_e} \approx 43$ times larger than the escaping flux of protons, thereby producing an unphysical net flux of negative charge from the Sun. Hence the electrostatic potential adjusts itself in order to confine the electrons well enough to keep their escaping flux equal to that of the protons. Broadly speaking, this positive polarization potential is a phenomenon similar to the charging of a space probe in an ionosphere; the space probe acquires a negative potential which repels the electrons since it would otherwise collect much more electrons than ions (in the ratio of their thermal velocities).

As in the case of space probes and for similar reasons, the potential at the base of the wind is of the order of several times the thermal energy for Maxwellian electrons. In the simple case of Maxwellian electrons and protons with equal temperature T_0 at the exobase r_0, one finds a potential $e\Phi(r_0) \approx 5k_BT_0$ (see section 4.5.2), which tends to accelerate the protons outward if it is larger than the modulus of the gravitational energy $\Phi_g(r_0) = m_pM_\odot G/r_0$ (where $M_\odot$ is the solar mass and G is the gravitational constant). With a typical temperature $T_0 \approx 1.5 \times 10^6$ K, this gives $\Phi(r_0) \approx 650$V, which corresponds to an energy nearly 4 times larger than the Pannekoek- Rosseland potential $\Phi_g(r_0)/2$, assuming a typical exobase radius $r_0 \approx 6r_\odot$ [*Lemaire and Scherer*, 1971]. It is worth noting that one can obtain an analytical expression of the corresponding wind terminal velocity V_{SW} from the approximate proton energy balance $m_pV_{SW}^2/2 \approx e\Phi(r_0) - \Phi_g(r_0)$, which gives $V_{SW} \approx 300$ km/s with the above parameters; (see sections 3.2 and 5.2 and a simplified derivation of N. Meyer-Vernet (A simple kinetic model of the solar wind, submitted to *American Journal of Physics*, 1998).

Contrary to the protons, which are all escaping, only the electrons of kinetic energy larger than $e\Phi(r_0)$ can escape from the exobase. It is therefore easy to understand why the possible presence of suprathermal electrons in the corona, which increases the electrostatic potential in order to prevent the electron flux to become larger than the proton flux, should increase the wind velocity as found numerically by *Maksimovic et al.* [1997a] and shown analytically in section 4. This kind of model emphasizes the role of the ambipolar potential in accelerating the wind, but, of course, the wind terminal velocity can be deduced equivalently from the energy input in the corona due to the electron heat flux (section 5). Note that such an exospheric model takes for granted a coronal temperature of the order of $1,000,000°$. *Scudder* [1992a, b] has suggested that this large temperature increase with respect to the value at the base of the transition region might be itself produced by velocity filtration in the attractive potential, due to the presence of suprathermal particles.

2.2. Moments of the Electron Velocity Distribution

We apply the formulation developed by *Lemaire and Scherer* [1971] to an arbitrary velocity distribution, using otherwise similar assumptions. Above the exobase, the electrostatic potential $\Phi(r)$ is assumed positive and monotonically decreasing, thereby attracting the electrons, and the magnetic field is assumed radial, i.e., the magnetic field at level r is $B(r) = \eta B(r_0)$ with $\eta = (r_0/r)^2$. We also assume as the above authors that no particles are coming from infinity, so that there are only three classes of populated orbits: (1) the escaping electrons that have enough kinetic energy to overcome the potential barrier; (2) the ballistic electrons that emerge from the exobase but cannot escape; (3) the elec-

trons trapped between two reflection points. In the complete absence of collisions, the latter orbits can be arbitrarily populated; thus to avoid introducing an ad hoc parameter, we assume as *Lemaire and Scherer* [1971] that these electrons are in quasi-equilibrium with those emerging from the exobase, so that their velocity distribution function is similar except for the different velocity range; this allows one to simplify considerably the calculations. Note that with typical parameters the escaping electrons turn out to represent a small fraction of the total density.

At a given altitude the nonescaping electrons (classes 2 and 3) have any pitch angle and speeds smaller than a maximum value given by

$$v_M = \left[2e\Phi(r)/m_e\right]^{1/2} \quad (1)$$

from energy conservation with the potential energy $-e\Phi(r)$, since the gravity is negligible. The case of the escaping particles is different: their speeds must satisfy $v > v_M$, but this is not the only condition. Indeed, at the exobase any electron with $v > v_M$ and a pitch angle smaller than $\pi/2$ will escape because of magnetic moment conservation; at distance r the conservation of energy and magnetic moment then requires that their pitch angles θ satisfy $0 < \theta < \theta_e$ with

$$\sin^2\theta_e = \eta\left(1 + V_e^2/v^2\right) \quad (2)$$

$$V_e = \left[\frac{2e}{m_e}\left(\Phi(r_0) - \Phi(r)\right)\right]^{1/2} \quad (3)$$

For accessible trajectories the velocity distribution $f_e(\mathbf{v})$ at distance r is given by Liouville's theorem in terms of the distribution $f_{e0}(\mathbf{v})$ at the exobase r_0, with conservation of particle energy and magnetic moment. Assuming for simplicity that the velocity distribution at the exobase is isotropic for each class of particles in the range of directions where it is not zero, this gives

$$f_e(\mathbf{v}) = f_{e0}\left(\sqrt{v^2 + V_e^2}\right) \quad (4)$$

where v is the velocity modulus and the above inequalities on v and θ are implied for each class of particles.

This allows one to calculate the scalar moments of the electron velocity distribution at altitude r as the sum of the contributions of the nonescaping and of the escaping electrons:

$$\begin{aligned} M_{eq} &= \int d^3v v^q f_e(v) \\ &= 4\pi\int_0^{v_M} dv v^{q+2} f_e(v) \\ &\quad + 2\pi\int_{v_M}^{\infty} dv v^{q+2} f_e(v)\int_0^{\theta_e} d\theta \sin\theta \end{aligned} \quad (5)$$

Substituting the distribution (4) and performing the angular integration, we obtain

$$\begin{aligned} M_{eq} &= 4\pi\int_0^{v_M} dv v^{q+2} f_{e0}\left(\sqrt{v^2 + V_e^2}\right) \\ &\quad + 2\pi\int_{v_M}^{\infty} dv v^{q+2} f_{e0}\left(\sqrt{v^2 + V_e^2}\right)\left(1 - \cos\theta_e\right) \end{aligned} \quad (6)$$

In contrast, the electron flux parallel to the magnetic field is given by the sole contribution of the escaping electrons, so that

$$\begin{aligned} F_e &= \int d^3v v_\parallel f_e(v) \\ &= 2\pi\int_{v_M}^{\infty} dv v^3 f_e(v)\int_0^{\theta_e} d\theta \sin\theta\cos\theta \end{aligned} \quad (7)$$

Substituting the distribution (4) and the expression (2) of θ_e, we deduce

$$F_e = \eta F \qquad F = \pi\int_{V_0}^{\infty} dv v^3 f_{e0}(v) \quad (8)$$

where we have introduced the notation $V_0 = \sqrt{V_e^2 + v_M^2}$, i.e.,

$$V_0 = \left[2e\Phi(r_0)/m_e\right]^{1/2} \quad (9)$$

The electron density at altitude r is $n_e = M_{e0}$ and the average electron temperature T_e, defined from the mean kinetic energy in the electron frame, is given by

$$3n_e k_B T_e = m_e\left[M_{e2} - F_e^2/n_e\right] \quad (10)$$

2.3. Moments of the Proton Velocity Distribution

The case of the protons is different. Owing to the gravitational attraction, they are subjected to the total potential $-m_p M_\odot G/r + e\Phi(r)$, which is assumed positive and monotonically decreasing above the exobase so that their velocity increases monotonically with altitude. All the protons present at altitude r are escaping, so that the accessibility from the exobase requires, from conservation of energy and magnetic moment, that their velocity and pitch angle satisfy $v > V_p$ and $0 < \theta < \theta_p$ with

$$\sin^2\theta_p = \eta\left(1 - V_p^2/v^2\right) \quad (11)$$

$$V_p^2 = \frac{2}{m_p}\{e\left[\Phi(r_0) - \Phi(r)\right] - \Phi_g(r_0) + \Phi_g(r)\} \quad (12)$$

$$\Phi_g(r) = m_p M_\odot G/r \quad (13)$$

If the proton velocity distribution at the exobase is $f_{p0}(\mathbf{v})$ (assumed isotropic in the range of directions where it is not zero, i.e., for $0 < \theta < \pi/2$), the distribution at altitude r for accessible trajectories is given from Liouville's theorem by

$$f_p(\mathbf{v}) = f_{p0}\left(\sqrt{v^2 - V_p^2}\right) \quad (14)$$

where the above inequalities on v and θ are implied. This allows one to calculate the scalar moments of the distribution at altitude r

$$\begin{aligned} M_{pq} &= \int d^3v v^q f_p(v) \\ &= 2\pi\int_{V_p}^{\infty} dv v^{q+2} f_{p0}\left(\sqrt{v^2 - V_p^2}\right)\left(1 - \cos\theta_p\right) \end{aligned} \quad (15)$$

The flux of protons parallel to the magnetic field is obtained in a similar way as for the electrons, using (14) and (11)

$$F_p = \pi\eta\int_0^{\infty} dv v^3 f_{p0}(v) \quad (16)$$

Contrary to the electron flux, the proton flux is independent

of the potential, which is not surprising since these particles are repelled.

2.4. Zero Electric Charge and Current

The electrostatic potential is calculated in a self-consistent way by writing (1) that there is no net flux of charge from the Sun; that is, $F_e = F_p$ and (2) that the plasma is everywhere approximatively neutral; that is, $n_e = n_p$.

The condition of zero net flux of charge yields from (8) and (16)

$$\int_{V_0}^{\infty} dv v^3 f_{e0}(v) = \int_0^{\infty} dv v^3 f_{p0}(v) \quad (17)$$

This equation determines the velocity V_0 and thus the electrostatic potential $\Phi(r_0)$ at the exobase as a function of the velocity distributions. It is important to note that whereas the solution depends on the whole proton velocity distribution $f_{p0}(v)$ at the exobase (from the right-hand side of (17)), it only depends on the high-energy part of the electron one, $f_{e0}(v > V_0)$ (left-hand side of (17)). Hence as already noted, the energetic electrons play an important role in the physics of the wind, but this is not the case for the protons.

The shape of the potential $\Phi(r)$ is calculated by writing the charge neutrality condition at any level r; that is, $M_{e0} = M_{p0}$, using (6) and (15). In general, this calculation has to be done iteratively; in this paper we use instead some simplifications valid at large distances in order to obtain an analytical result.

Note that the normalization of the distributions $f_{e0}(v)$ and $f_{p0}(v)$ is determined by the charge neutrality condition at r_0, which can be written since $\theta_e = \theta_p = \pi/2$ and $v_M = V_0$ at r_0

$$n_e(r_0) = 4\pi \int_0^{\infty} dv v^2 f_{e0}(v) - 2\pi \int_{V_0}^{\infty} dv v^2 f_{e0}(v) \quad (18)$$

$$n_e(r_0) = n_p(r_0) = 2\pi \int_0^{\infty} dv v^2 f_{p0}(v) \quad (19)$$

In practice, the second integral in (18) is much smaller than the first one since V_0 is generally much larger than the most probable speed of the distribution $f_{e0}(v)$; hence $n_e(r_0)$ is roughly equal to the integral of $f_{e0}(v)$ over the whole velocity space. In contrast, $n_p(r_0)$ given by (19) is half the integral of $f_{p0}(v)$ over the whole velocity space, which comes from the fact that there are no protons coming inward.

3. General Expressions at Large Distances

3.1. Generic Electron Temperature Radial Profile

In order to obtain analytical expressions, we now consider large distances; that is, $\eta = (r_0/r)^2 \ll 1$. In this case, the velocities V_e and V_p given in (3) and (12), respectively, can be approximated by

$$V_e \approx [2e\Phi(r_0)/m_e]^{1/2} \equiv V_0 \quad (20)$$

$$V_p \approx \left\{\frac{2}{m_p}[e\Phi(r_0) - \Phi_g(r_0)]\right\}^{1/2} \equiv V_{p0} \quad (21)$$

The proton moments (15) can be simplified by writing $1 - \cos\theta_p \approx \eta\left(1 - V_p^2/v^2\right)/2$ (from (11) with $\theta_p \ll 1$), substituting $V_p \approx V_{p0}$, and making a change of variable in the integral, so that

$$M_{pq} \approx C_q \eta \quad (22)$$

$$C_q = \pi \int_0^{\infty} dv \frac{v^3}{\left(v^2 + V_{p0}^2\right)^{(1-q)/2}} f_{p0}(v) \quad (23)$$

Hence in this approximation all the proton scalar moments vary as η at large distances, so that the average proton temperature, which is given by an equation similar to (10), is a constant. This represents the contribution of their parallel temperature, which follows approximatcly a double-adiabatic equation at large distances, whereas their perpendicular temperature is much smaller [*Lemaire and Scherer*, 1972].

We concentrate here on the electron moments. They can be simplified in a similar way by substituting the expression (2) of θ_e with $\theta_e \ll 1$ into the expression (6) of M_{eq}, so that

$$M_{eq} \approx 4\pi \int_0^{v_M} dv v^{q+2} f_{e0}\left(\sqrt{v^2 + V_0^2}\right) + \pi\eta \int_{v_M}^{\infty} dv v^q f_{e0}\left(\sqrt{v^2 + V_0^2}\right)\left(v^2 + V_0^2\right) \quad (24)$$

Furthermore, v_M is generally much smaller than the scale of the variation of the distribution $f_{e0}(v)$; (this can be verified a posteriori). Since we have also $v_M \ll V_0$, we can make the approximation

$$f_{e0}\left(\sqrt{v^2 + V_0^2}\right) \approx f_{e0}(V_0)$$

in the range $0 < v < v_M$, so that the first term of the sum in (24) can be approximated by

$$4\pi f_{e0}(V_0) \int_0^{v_M} dv v^{q+2} = \frac{4\pi}{q+3} f_{e0}(V_0) v_M^{q+3} \quad (25)$$

For the same reason, in the second term of M_{eq} the integral $\int_{v_M}^{\infty}$ can be approximated by $\int_0^{\infty}$ because the contribution of the range of integration $0 < v < v_M$ is small. Hence the electron scalar moments M_{eq} can be written

$$M_{eq} \approx 4\pi f_{e0}(V_0) v_M^{q+3}/(q+3) + \pi\eta \int_0^{\infty} dv v^q f_{e0}\left(\sqrt{v^2 + V_0^2}\right)\left(v^2 + V_0^2\right) \quad (26)$$

Thus in this approximation all the electron scalar moments vary with distance as

$$M_{eq} \approx D_q v_M^{q+3} + B_q \eta \quad (27)$$

$$D_q = 4\pi f_{e0}(V_0)/(q+3) \quad (28)$$

$$B_q = \pi \int_{V_0}^{\infty} dv v^3 \left(v^2 - V_0^2\right)^{(q-1)/2} f_{e0}(v) \quad (29)$$

where the first and second terms of the sum (27) stem from the nonescaping and the escaping electrons, respectively.

We now write the neutrality condition $n_e = n_p$ at large

distances; that is, $M_{e0} = M_{p0}$ which reads, using (27) and (22)

$$n_e = n_p \approx D_0 v_M^3 + B_0 \eta \approx C_0 \eta \quad (30)$$

when

$$v_M \approx [\eta (C_0 - B_0)/D_0]^{1/3} \quad (31)$$

This can be further simplified by noting that the contribution of the escaping electrons to the total density is small, i.e., $B_0 \ll C_0$; (this will be verified a posteriori). An important consequence is that the electrostatic potential at large distances $\Phi(r) = m_e v_M^2/2e$ is given explicitly by

$$\Phi(r) \approx m_e [\eta C_0/D_0]^{2/3}/2e \quad (32)$$

which varies as $\Phi(r) \propto \eta^{2/3} \propto 1/r^{4/3}$.

The electron temperature is deduced by substituting into (10) the electron moment M_{e2} given in (27), the electron flux F_e given in (8), and the density given in (30), using the expression (31) of v_M with $B_0 \ll C_0$. Noting that in (10) we can neglect the electron flux term since the wind velocity $V_{SW} = F_e/n_e = F/C_0$ is generally much smaller than the electron thermal velocity (this will also be verified a posteriori), and using $D_2/D_0 = 3/5$ (from (28)), the electron temperature is finally given by

$$T_e = T_{4/3} + T \quad (33)$$

where $T_{4/3}$, which comes from the first term in (27), is directly related to the electric potential by

$$T_{4/3} \approx \frac{2e\Phi(r)}{5k_B} \quad (34)$$

$$T_{4/3} \approx \frac{m_e}{5k_B}\left(\frac{C_0}{D_0}\right)^{2/3} \eta^{2/3} \quad (35)$$

and T, which comes from the second term in (27), is a constant given by

$$T \approx \frac{m_e B_2}{3k_B C_0} \quad (36)$$

This is an important result; without specifying the velocity distributions, we find that the electron temperature at large distances is the sum of a term varying as $\eta^{2/3} \propto 1/r^{4/3}$ plus a constant.

It may be worth noting that the behavior at short distances is very different. Indeed just above the exobase, the expression (6) of the moments M_{eq} can be simplified differently since in that case $V_e \ll v_M \sim V_0$. Hence if V_0 is larger than the scale of variation of the velocity distribution, one finds instead of (26): $M_{eq} \approx 4\pi \int_0^\infty dv v^{q+2} f_{e0}\left(\sqrt{v^2 + V_e^2}\right)$. As a consequence, if f_{e0} is a Maxwellian, the term involving V_e^2, which determines the variation with distance, factorizes and can be put outside the integral, so that M_{e0} and M_{e2} vary similarly with distance, and the temperature is thus a constant just above r_0. In contrast, if f_{e0} has a suprathermal tail, being, for example, a Kappa function, then M_{e2} decreases less quickly with distance than M_{e0} (because of the weighting factor v^{q+2}), so that just above the exobase, the temperature increases with altitude [see *Scudder*, 1992a; *Meyer-Vernet et al.*, 1995].

3.2. Order-of-Magnitude Evaluation

What are the relative importance of the two terms $T_{4/3}$ and T in the electron temperature (33) at large distance? In this section we make order-of-magnitude estimates (indicated by the symbol $\sim$) in the spirit of the methods described, for example, by *Migdal* [1977]. We have

$$T_{4/3}/T = \frac{3C_0^{5/3}}{5D_0^{2/3}B_2}\eta^{2/3} \quad (37)$$

The constant C_0 given in (23), which determines the density since $n_p = C_0\eta$, and the proton flux (16) can be estimated by noting that the integrals in these expressions are determined by the bulk of the proton distribution $f_{p0}(v)$. Hence they can be evaluated by approximating this distribution with a function decreasing at the scale w_p, as does, for example, a Maxwellian of thermal velocity w_p. We also assume that $V_{p0} > w_p$, which can be, in practice, verified a posteriori, since V_{p0} is roughly the terminal wind velocity. In this case, the square root in the expression (23) of C_0 can be replaced by V_{p0} to obtain an order-of-magnitude estimate, so that, comparing with the flux (16), we find

$$C_0 \sim F_p/(\eta V_{p0}) \quad (38)$$

Note that the terminal wind velocity is $V_{SW} = F_p/n_p = F_p/(\eta C_0)$; that is,

$$V_{SW} \sim V_{p0} = \left\{\frac{2}{m_p}[e\Phi(r_0) - \Phi_g(r_0)]\right\}^{1/2} \quad (39)$$

as expected from the proton energy balance when the terminal wind velocity is large compared to the proton thermal, bulk velocity and heat flux terms at the exobase (see also section 5.2).

In contrast, the integrals contained in the expressions concerning the electrons involve the high-velocity range ($v > V_0$) of the electron distribution. For V_0 much larger than the scale of variation of this distribution, most contributions to the integrals in (29) and (8) occur in the vicinity of $v \sim V_0$ with a range of integration of order V_0, so that in order of magnitude

$$B_q \sim \pi f_{e0}(V_0) V_0^{q+3} \quad (40)$$

$$F_e/\eta = F \sim \pi f_{e0}(V_0) V_0^4 \quad (41)$$

Equalizing the electron flux F_e given from (41) and the proton flux F_p given from (38), we thus obtain

$$C_0 V_{p0} \sim \pi f_{e0}(V_0) V_0^4 \quad (42)$$

We deduce the ratio of the two temperature terms by substituting (28), (40), and (42) with the relevant values of q into (37) and using the order-of-magnitude relation $V_0/V_{p0} \sim (m_p/m_e)^{1/2}$ (from (20) and (21))

$$T_{4/3}/T \sim 0.5\,(m_p/m_e)^{5/6}\,(r_0/r)^{4/3} \quad (43)$$

Expressing the distance r in astronomical units (1.5×10^{11} m) and the exobase radius r_0 in solar radii ($r_\odot = 7 \times 10^8$ m), we finally obtain the electron temperature order-of-magnitude profile

$$T_e(r) \propto \sim 0.2\left(\frac{r_{0(r_\odot)}}{r_{(\mathrm{AU})}}\right)^{4/3} + 1 \quad (44)$$

Since the exobase is typically at a few solar radii, the electron temperature profile is the sum of a $r^{-4/3}$ term plus a constant, with both terms of the same order of magnitude at 1 AU. The $r^{-4/3}$ term comes from the first term of (26), i.e., from the nonescaping electrons which are isotropically distributed. In contrast, the constant stems from the second term in the sum (26), i.e., from the escaping electrons. Since, for them, $\theta < \theta_e$, we have for $\eta \ll 1$: $v_\perp^2/v^2 = \sin^2\theta < \eta\left(1 + V_0^2/v^2\right)$, so that it can be easily shown that their perpendicular temperature is negligible at large distances (by a factor of order η). The constant temperature term is thus the contribution of the parallel temperature of the escaping electrons.

Note that in order to simplify the electron temperature, we have assumed that the fractional contribution B_0/C_0 of the escaping electrons to the total electron density at large distances is small. This is justified since from (40) and (42); this contribution is given by: $B_0/C_0 \sim V_{p0}/V_0 \sim (m_e/m_p)^{1/2}$, i.e., a few percent; note that this value is independent of distance. We have also assumed that the particle flux term is negligible in the expression (10) of the electron temperature, i.e., $F^2/C_0 \ll B_2$. This inequality is verified since (40) and (41) yield $F^2/B_2 \sim B_0$. Finally, the large distance approximation was mainly based on the inequality $v_M \ll V_0$. Substituting (28) and (42) into (31), we find $(v_M/V_0)^3 \sim 3\eta\,(m_p/m_e)^{1/2}/4$, so that the large distance approximation requires $(r_0/r)^2 \ll 4\,(m_e/m_p)^{1/2}/3 \sim 0.03$.

It is important to note that the order-of-magnitude profile (44) is generic since it has been obtained with very weak hypotheses on the velocity distributions at the exobase. In the following sections, we specify these distributions.

4. Application to a Kappa Electron Velocity Distribution

Since, as already noted, the moments of the proton velocity distribution depend on the bulk of the distribution at the exobase, the results are not expected to be drastically changed by the presence of suprathermal protons at this level. We thus assume hereafter that they are Maxwellian distributed at the exobase.

4.1. Maxwellian Proton Velocity Distribution

The Maxwellian velocity distribution of thermal velocity w_p is given by

$$f_{p0}(v) = \frac{n_{p0}}{\pi^{3/2} w_p^3} e^{-v^2/w_p^2} \quad (45)$$

The normalization constant n_{p0} is determined by (19), which gives

$$n_p(r_0) = n_{p0}/2 \quad (46)$$

(as already noted, the factor 1/2 is due to the fact that there are only escaping protons, i.e., one half of an isotropic distribution $f_{p0}(v)$). Hence the proton flux (16) is given by

$$F_p = \eta n_p(r_0)\, w_p/\sqrt{\pi} \quad (47)$$

and the expression (23) of C_0 yields (with the normalization (46))

$$C_0 \equiv n_p(r)/\eta = n_p(r_0)\,\frac{P\left(\sqrt{U_{p0}}\right)}{\sqrt{\pi}} \quad (48)$$

$$U_{p0} = V_{p0}^2/w_p^2 \quad (49)$$

$$\frac{P(x)}{\sqrt{\pi}} = \left(\frac{1}{2} - x^2\right) e^{x^2}\left[1 - erf(x)\right] + \frac{x}{\sqrt{\pi}} \quad (50)$$

as found by *Lemaire and Scherer* [1971]. If $x > 1$, we have

$$P(x) \approx \left(1 - 1/x^2 + 9/4x^4 - 15/2x^6 + \ldots\right)/x \quad (51)$$

The terminal wind velocity is deduced by dividing the proton flux (47) by the density given in (48)

$$V_{SW} = F_p/n_p = w_p/P\left(\sqrt{U_{p0}}\right) \quad (52)$$

If $U_{p0} \gg 1$, this yields, from (51), $V_{SW} \approx V_{p0}$. The velocity V_{p0}, defined in (21) depends on the potential $\Phi(r_0)$ at the exobase, which, in turn, depends on the electron velocity distribution $f_{e0}(v)$. In the next section we consider a Kappa electron velocity distribution, which generalizes the Maxwellian by including a suprathermal tail.

4.2. Kappa Electron Velocity Distribution

This kind of electron velocity distribution in the corona has been considered, in particular, by *Scudder* [1992a, b] and numerically by *Maksimovic et al.* [1997a]. Namely,

$$f_{e0}(v) = \frac{n_{e0}}{2\pi}\frac{A_\kappa}{\left(\kappa w_e^2\right)^{3/2}}\left[1 + \frac{v^2}{\kappa w_e^2}\right]^{-(\kappa+1)} \quad (53)$$

$$A_\kappa = \frac{\Gamma(\kappa+1)}{\Gamma(\kappa - 1/2)\,\Gamma(3/2)} \quad (54)$$

This function is rather close to a Maxwellian of temperature $m_e w_e^2/2k_B$ at low energies and has the same most probable speed, but it has a suprathermal tail whose contribution decreases as κ increases, with the distribution approaching a Maxwellian as $\kappa \to \infty$ since $A_\kappa \to 2\kappa^{3/2}/\sqrt{\pi}$ and $\left(1 + v^2/\kappa w_e^2\right)^{-(\kappa+1)} \to e^{-v^2/w_e^2}$. This function might be suitable to describe electron velocity distributions in the solar wind, where suprathermal electrons with a power law spectrum have been detected over a large energy range [*Lin*, 1997], and it has indeed been recently used to fit measured solar wind electron distributions [*Maksimovic et al.*, 1997b]. *Roberts* [1998] suggested recently that turbulent waves can produce a suprathermal electron tail at the base of the transition region, but the presence of a Kappa electron distribu-

tion in the corona is still subject to some debate [*Ko et al.*, 1996]. We introduce the notations

$$T_{e0} \equiv m_e w_e^2/2k_B; \quad T_{p0} \equiv m_p w_p^2/2k_B \quad (55)$$

$$t \equiv T_{e0}/T_{p0} \quad (56)$$

$$\mu \equiv w_p/w_e \equiv \left(\frac{m_e}{m_p t}\right)^{1/2} \quad (57)$$

$$U_0 \equiv V_0^2/w_e^2 \equiv e\Phi(r_0)/k_B T_{e0} \quad (58)$$

so that (20), (21), and (49) yield

$$\frac{U_{p0}}{tU_0} = 1 - \frac{\Phi_g(r_0)}{U_0 k_B T_{e0}} \equiv \alpha \quad (59)$$

where α has been assumed to be positive (see section 2), which can be verified a posteriori; note also that the simplifications made in section 3.1 assume implicitly that $v_M < w_e$, which can also be verified a posteriori since $v_M/w_e \approx (5T_{4/3}/2T_{e0})^{1/2}$. Note that from section 4.1, when the terminal wind velocity is large compared to the proton thermal velocity at the exobase, we have

$$V_{SW} \approx V_{p0} \approx w_e\sqrt{m_e\alpha U_0/m_p} \quad (60)$$

With the above Kappa distribution, the electron flux at any distance given in (8) reduces to

$$F_e(r) = \eta\frac{n_{e0}A_\kappa w_e}{4\sqrt{\kappa}(\kappa-1)}\left[1+\frac{U_0}{\kappa}\right]^{-\kappa}[1+U_0] \quad (61)$$

as found by *Pierrard and Lemaire* [1996]. Equalizing this flux to the proton flux (47), we obtain U_0 as solution of

$$\left[1+\frac{U_0}{\kappa}\right]^{-\kappa}(1+U_0) = \mu\frac{4n_p(r_0)}{\sqrt{\pi}n_{e0}}\frac{\sqrt{\kappa}(\kappa-1)}{A_\kappa} \quad (62)$$

The normalization parameter n_{e0} is calculated from the charge neutrality condition at the exobase (18)-(19). With the Kappa distribution (53) this yields

$$n_e(r_0) = n_{e0}\left[1-\frac{1}{2}\beta_2\left(\frac{1}{1+U_0/\kappa}\right)\right] = n_p(r_0) \quad (63)$$

$$\beta_2(y) = A_\kappa\int_0^y dx x^{\kappa-3/2}(1-x)^{1/2} \quad (64)$$

The parameters D_q and B_q involved in the electron moments are calculated in the appendix. Substituting (48), (A1), and (A4) into (36) and (35) and using (62), we deduce the two terms of the electron temperature at large distances $T_e \equiv T_{4/3} + T$ as

$$\frac{T_{4/3}}{T_{e0}} = \frac{1}{10}\left[\frac{3\eta P}{\mu}\frac{\kappa}{\kappa-1}\left(1+\frac{U_0}{\kappa}\right)(1+U_0)\right]^{2/3} \quad (65)$$

$$\frac{T}{T_{e0}} = \frac{2\mu\kappa^{3/2}(\kappa-1)(U_0+3/2)}{3PA_\kappa(\kappa-3/2)(U_0+1)}\left(1+\frac{U_0}{\kappa}\right)^{1/2} \quad (66)$$

(These results can be retrieved by making a tedious asymptotic expansion of the formulae given by *Pierrard and Lemaire* [1996] and summing on the different classes of orbits.) Note that the fractional contribution of the escaping electrons to the density is B_0/C_0 given by (A3), (48), and (62), as

$$\frac{n_{esc}}{n_e} \approx \frac{\mu}{P}\frac{2\sqrt{\kappa}(\kappa-1)(U_0+1/2)}{A_\kappa(U_0+1)(1+U_0/\kappa)^{1/2}} \quad (67)$$

These expressions simplify in several cases studied below.

4.3. Maxwellian Electrons ($\kappa \to \infty$)

Letting $\kappa \to \infty$ in the above equations, we obtain

$$\frac{T_e}{T_{e0}} \approx \frac{1}{10}\left[\frac{3\eta P}{\mu}(1+U_0)\right]^{2/3} + \frac{\sqrt{\pi}\mu}{3P}\frac{U_0+3/2}{U_0+1} \quad (68)$$

The fractional contribution (67) of the escaping electrons to the density is $n_{esc}/n_e \approx (\sqrt{\pi}\mu/P)(U_0+1/2)/(U_0+1)$. In addition, (62), which allows one to calculate U_0, reduces to

$$(1+U_0)e^{-U_0} = 2\mu n_p(r_0)/n_{e0} \quad (69)$$

where the right-hand side member is deduced from $n_e(r_0) = n_p(r_0)$ with, from (63),

$$\frac{n_e(r_0)}{n_{e0}} = \frac{1}{2}\left[1+erf\left(\sqrt{U_0}\right)\right] - \sqrt{\frac{U_0}{\pi}}e^{-U_0} \quad (70)$$

as found by *Lemaire and Scherer* [1971].

If $U_0 \gg 1$, these expressions further simplify to give

$$T_e \approx T_{e0}\left[\frac{1}{10}\left(\frac{3\eta P U_0}{\mu}\right)^{2/3} + \frac{\sqrt{\pi}}{3}\frac{\mu}{P}\right] \quad (71)$$

and $n_e(r_0) \approx n_{e0}$ (with a relative error of $\sqrt{U_0/\pi}e^{-U_0}$) so that U_0 is now given by $(1+U_0)e^{-U_0} \approx 2\mu$. If in addition $U_{p0} \equiv V_{p0}/w_p \gg 1$, we have $P \approx 1/\sqrt{U_{p0}}$, so that the ratio of the two terms in the electron temperature is

$$\frac{T_{4/3}}{T} \approx 0.35\ \eta^{2/3}\left(\frac{m_p}{m_e\alpha}\right)^{5/6}U_0^{-1/6} \quad (72)$$

where α, defined in (59), is of order 1 or smaller, and we have $n_{esc}/n_e \approx (\pi\alpha U_0 m_e/m_p)^{1/2}$. With typical parameters, (69) yields $U_0 \approx 4-6$, so that $T_{4/3}/T \approx 0.27\ \eta^{2/3}(m_p/\alpha m_e)^{5/6}$ and $n_{esc}/n_e \approx 0.08\sqrt{\alpha}$. However, with these moderate values of U_0, the above approximations are rather rough.

4.4. Large Potential With Finite Kappa ($\kappa \ll U_0$)

Consider now the case $U_0 \gg \kappa$. Equation (63) reduces to $n_e(r_0) \approx n_{e0}$ (with a relative error of $A_\kappa/(2\kappa-1)\times(\kappa/U_0)^{\kappa-1/2}$), and (62) yields

$$U_0 \approx \left[\frac{\sqrt{\pi}A_\kappa\kappa^{\kappa-1/2}}{4\mu(\kappa-1)}\right]^{1/(\kappa-1)} \quad (73)$$

so that the normalized electrostatic potential increases as κ

decreases, as expected since the presence of suprathermal electrons tends to increase the electron flux. The electron temperature given in (65) and (66) reduces to

$$\frac{T_e}{T_{e0}} \approx \frac{1}{10}\left(\frac{3\eta P U_0^2}{\mu(\kappa-1)}\right)^{2/3} + \frac{2\mu\kappa(\kappa-1)U_0^{1/2}}{3PA_\kappa(\kappa-3/2)} \quad (74)$$

If, in addition, $U_{p0} \equiv V_{p0}/w_p \gg 1$, which is generally true when $U_0 \gg \kappa$, we have $P \approx 1/\sqrt{U_{p0}}$ so that the ratio of the two temperature terms is

$$\frac{T_{4/3}}{T} \approx 0.31\eta^{2/3}\left(\frac{m_p}{m_e\alpha}\right)^{5/6}\left[\frac{A_\kappa(\kappa-3/2)}{\kappa(\kappa-1)^{5/3}}\right] \quad (75)$$

with α still given in (59), i.e., of order 1 or smaller. This yields $T_{4/3}/T \approx 0.21\eta^{2/3}(m_p/m_e\alpha)^{5/6}$ (within 5%) for Kappa varying from 2 to 6. Note that in this case (67) gives $n_{esc}/n_e \approx 2\kappa A_\kappa^{-1}(\kappa-1)\sqrt{m_e\alpha/m_p}$, so that $n_{esc}/n_e \approx (0.04-0.09)\sqrt{\alpha}$ for $\kappa = 2-6$. The smaller is κ, the larger is U_0, and the closer is α to 1 (in particular, for $\kappa \leq 3$, $\alpha \approx 1$.)

4.5. Applications

4.5.1 General approximate results.. Since the ratio of the two temperature terms, $T_{4/3}/T$ as a function of η, varies weakly in the two extreme cases considered above and, as shown below, we have, in practice, $\alpha \approx 0.5-1$, we find that the electron temperature radial profile can be approximated by

$$T_e \propto 0.13\left(\frac{r_{0(r_\odot)}}{r_{(AU)}}\right)^{4/3} + 1 \quad (76)$$

over a large range of parameters; here r_0 is in $r_\odot$ and r in AU. We will see indeed that this expression is very close to the more accurate results obtained in the following sections. The above expression refines the order-of-magnitude estimate obtained in section 3.2 without specifying the velocity distributions in the corona and confirms that the shape of the electron temperature radial profile is weakly dependent on these velocity distributions. As an illustration, we have plotted in Figure 1 the profiles obtained between 0.3 and 5 AU with $r_0 = 6\ r_\odot$ and $r_0 = 3\ r_\odot$, which are reasonable values in the so-called quiet corona and a coronal hole, respectively (see sections 4.5.2 and 4.5.3); we have superimposed some power law approximations, close to values used to fit measured profiles of the average electron temperature [*Marsch et al.*, 1989] or of its components [*Pilipp et al.*, 1990].

In contrast, the terminal wind velocity V_{SW} and the absolute value of the electron density and temperature do depend on the electron velocity distribution at the exobase. Indeed the normalized potential U_0 cannot be extremely large with a Maxwellian electron distribution because of the exponential factor in (69). An order of magnitude can be obtained in this case by using (60) with $U_0 \approx 5$ and $\alpha \lesssim 1$, which yields $V_{SW} \lesssim 5 \times 10^{-2} w_e$, i.e., $V_{SW} \lesssim 300\sqrt{T_{e0}}$ (in SI units). This is no longer true when the distribution decreases less steeply at high energies. With a Kappa distribution the terminal velocity is approximately given by (60), so that from (59) and (73) we have for a large normalized potential $U_0 \gg \kappa$

$$V_{SW} \approx w_e\sqrt{\frac{m_e}{m_p}}\left\{\left[\frac{w_e}{w_p}\frac{\sqrt{\pi}A_\kappa\kappa^{\kappa-1/2}}{4(\kappa-1)}\right]^{1/(\kappa-1)} - \frac{\Phi_g(r_0)}{k_B T_{e0}}\right\}^{1/2} \quad (77)$$

Since the main variation comes from the factor $(w_e/w_p)^{\frac{1}{\kappa-1}}$ the velocity V_{SW} increases as κ decreases, i.e., as the exobase electron velocity distribution has more suprathermal electrons. For example, with $t \approx 1$ and $\kappa \approx 2-3$ (for which the second term in the curled bracket above can be neglected, in practice), (77) yields $V_{SW} \approx [0.27-0.13]\,w_e$; that is, $V_{SW} \approx [1500-700]\sqrt{T_{e0}}$ in SI units. Note that the density at large distances $n_p(r) \approx n_p(r_0)\,\eta w_p \pi^{-1/2}/V_{SW}$ varies in the opposite sense. We consider below two illustrative cases without using the approximation of a large potential.

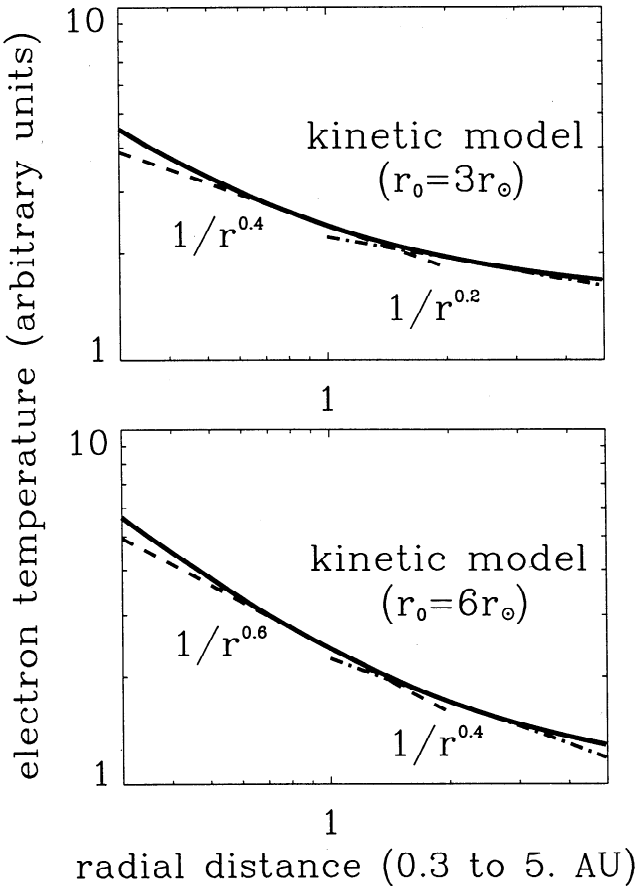

Figure 1. Large-distance radial profiles of the average electron temperature obtained analytically using a collisionless kinetic model of the solar wind with an exobase radius of (top) $3r_\odot$ and (bottom) $6r_\odot$. Power law approximations have been drawn for comparison.

4.5.2 An illustrative case study with Maxwellian electrons.. With a Maxwellian electron distribution at the exobase and assuming, for simplicity, that $t \equiv T_{e0}/T_{p0} \approx 1$ so that $\mu \approx \sqrt{m_e/m_p}$, we deduce from (69) and (70): $U_0 \approx 4.8$. With the solar mass $M_\odot \approx 2 \times 10^{30}$ kg we obtain $U_{p0} \approx U_0 - 2.3 \times 10^7/\left(r_{0(r_\odot)} T_{e0}\right)$; hence the existence of a wind requires in this case: $r_{0(r_\odot)} T_{e0} > 4.8 \times 10^6$ K, i.e., not too small an exobase radius and/or temperature.

The exobase r_0 is evaluated as the radius where the mean collisional free path equals the scale height, which gives different exobase radii for the electrons and protons since they have different mean free paths. However, this difference can be neglected because the variation in free path translates into a small variation in r_0, owing to the large density gradient in the corona.

Let us consider parameter values typical for the so-called "quiet" corona, which may be a source for the slow wind. With the density profile given by *Withbroe* [1988] and assuming $T_{p0} \approx T_{e0} \approx 1.5 \times 10^6$ K at a few solar radii, we find an exobase radius $r_0 \approx 6 r_\odot$. Note that T_{e0} and T_{p0} defined by (55) are rather close to the values of the electron and proton temperatures at the exobase calculated from (10) and a similar equation for the protons, respectively, by integrating the distributions in velocity space [*Lemaire and Scherer*, 1972] (note also that the corresponding flow speed at the exobase is, from (47), $w_p/\sqrt{\pi} \approx 90$ km/s). With these parameters the electron average temperature profile (68), terminal velocity (52), and density (48) at large distances are

$$\begin{aligned} T_e(r) &\approx 4.4 \times 10^4 \left[1.5/r_{\mathrm{AU}}^{4/3} + 1\right] \quad \mathrm{K} \\ V_{\mathrm{SW}} &\approx 314 \quad \mathrm{km/s} \\ n_p(r) &\approx 13/r_{\mathrm{AU}}^2 \quad \mathrm{cm}^{-3} \end{aligned} \tag{78}$$

These values, obtained analytically, agree with the numerical results of *Lemaire and Scherer* [1971] and are in the range of observations in the slow wind [see *Schwenn and Marsch*, 1991 and references therein]. In particular, a power law fitting of the radial profile of the average electron temperature measured between 0.3 and 1 AU yields an index $\beta \approx [0.4 - 0.66]$ in this type of wind [*Marsch et al.*, 1989], which is a reasonable approximation of the profile above (see Figure 1, bottom).

4.5.3 An illustrative case study with a Kappa electron distribution.. As already noted, with a Kappa electron distribution the normalized potential U_0 increases as κ decreases, which may produce a large terminal velocity. Hence let us consider parameters relevant for a so-called polar "coronal hole," which is believed to be a source for high-speed wind, and assume, for illustrative purposes, $\kappa = 3$, which yields $U_0 \approx 28$ in the simple case where $T_{e0} = T_{p0}$. With such a large value of U_0, U_{p0} depends weakly on r_0 and T_{e0} and the existence of a wind requires $r_0 T_{e0} > 0.8 \times 10^6$ K, which is a much weaker condition than with a Maxwellian.

To evaluate the exobase radius, we use the density profile given by *Withbroe* [1988] for a polar coronal hole near the minimum of the solar cycle, which lies within a factor of 2 of recent observations [*Fisher and Guhathakurta*, 1995]. There is a large uncertainty on the coronal hole temperatures and no overall agreement [see, for example, *Habbal et al.*, 1993; *Ko et al.*, 1997; *David et al.*, 1997], especially in the outer corona, and we assume, for simplicity, $T_{e0} \approx T_{p0} \approx 10^6$ K at a few solar radii, which yields $r_0 \approx 3\, r_\odot$.

We deduce the electron average temperature profile from (65) and (66), the terminal wind velocity from (52) using (59), and the density from (48)

$$\begin{aligned} T_e(r) &\approx 3 \times 10^5 \left[0.55/r_{\mathrm{AU}}^{4/3} + 1\right] \quad \mathrm{K} \\ V_{\mathrm{SW}} &\approx 610 \quad \mathrm{km/s} \\ n_p(r) &\approx 2/r_{\mathrm{AU}}^2 \quad \mathrm{cm}^{-3} \end{aligned} \tag{79}$$

Note that these results are close to those given by the simplified expressions (73), (74), and (77), which represent very good approximations in this case. The velocity is in the low range of high-speed values and the density is compatible with observations in the fast polar wind near solar minimum [*Phillips et al.*, 1995; *Issautier et al.*, 1997]. A power law fitting of the radial profile of the average electron temperature measured between 0.3 and 1 AU yields a mean index $\beta \approx [0.15 - 0.48]$ (including the error bars) in high-speed wind [*Marsch et al.*, 1989], with a tendency of the profiles to steepen with decreasing distance [*Pilipp et al.*, 1990]; this is in reasonable agreement with the profile above (see Figure 1, top). However, the temperature value is more than twice larger than that typically observed in this type of wind [see *Pilipp et al.*, 1990]. Assuming larger thermal temperatures at the exobase and/or a smaller value of Kappa increases the terminal velocity (see(77)) but also increases the discrepancy in the temperature at large distances. One can also verify from (74) that this discrepancy cannot be resolved by assuming a smaller thermal electron temperature and/or a larger proton temperature in the corona, as suggested by some recent observations [see, for example, *Kohl et al.*, 1996; *David et al.*, 1997] (see also section 6).

5. Momentum and Energy Balance

5.1. Electron Fluid Equations

Do our results agree with the fluid equations? Since the electron temperature is anisotropic, one must use the anisotropic fluid equations. The radial momentum equation for the electrons in a radial magnetic field reads

$$e\frac{d\Phi}{dr} = \frac{1}{n_e}\frac{d}{dr}\left(n_e k_B T_{e\|}\right) + \frac{2}{r} k_B \left(T_{e\|} - T_{e\perp}\right) \tag{80}$$

$$e\frac{d\Phi}{dr} = \frac{d}{dr} k_B T_{e\|} - \frac{2}{r} k_B T_{e\perp} \tag{81}$$

where we have neglected the electron inertia and gravitational terms, assumed the pressure tensor diagonal with $T_{e\|}$ and $T_{e\perp}$ the parallel and perpendicular electron temperatures, respectively, and $n_e \propto 1/r^2$. Since the average electron temperature at large distances is the sum of a term $T_{4/3}$ coming from the nonescaping electrons, which have equal parallel and perpendicular temperatures, plus a constant coming from the parallel temperature of the escaping electrons (whose perpendicular temperature is negligible),

with the fractional contributions of these two components to the total density being constants, we have $T_{e\perp} = T_{4/3}$ and $dT_{e\parallel}/dr = dT_{4/3}/dr$. Hence (81) yields

$$e\frac{d\Phi}{dr} = k_B\left(\frac{dT_{4/3}}{dr} - \frac{2}{r}T_{4/3}\right) \quad (82)$$

With $T_{4/3} \propto r^{-4/3}$, this gives $e\Phi(r) \approx (5/2)\,k_B T_{4/3}$, which agrees with (34).

Note that in contrast, the isotropic fluid radial momentum balance equation would give incorrect results, which is not surprising. Indeed writing instead of (80)

$$e\frac{d\Phi}{dr} = \frac{1}{n_e}\frac{d}{dr}\left(n_e k_B T_e\right) \quad (83)$$

with $n_e \propto r^{-2}$, $T_e = T_{4/3} + T$ with $T_{4/3} \propto \Phi \propto r^{-4/3}$ and T being a constant, we find $ed\Phi/dr = -2k_B \times \left[(5/3)\,T_{4/3} + T\right]/r$, which is not compatible with (34).

One would also like to retrieve the $r^{-4/3}$ variation of the term $T_{4/3}$ from the anisotropic fluid energy equation for the electrons. This equation reads

$$\frac{d}{dr}\left[\frac{k_B}{2}\left(T_{e\parallel} + 2T_{e\perp}\right) + \frac{Q_{e\parallel}}{F_e}\right] + \frac{2}{r}k_B T_{e\perp} = 0 \quad (84)$$

with a radial magnetic field and $n_e \propto r^{-2}$. Since the parallel electron heat flux at large distances $Q_{e\parallel} \propto r^{-2}$ (from (87)), i.e., varies as the particle flux F_e, this reduces to

$$\frac{d}{dr}\left(\frac{T_{e\parallel}}{2} + T_{e\perp}\right) + \frac{2}{r}T_{e\perp} = 0 \quad (85)$$

With $T_{e\perp} = T_{4/3}$ and $dT_{e\parallel}/dr = dT_{4/3}/dr$, this gives $dT_{4/3}/dr = -(4/3)\,T_{4/3}/r$, which yields indeed $T_{4/3} \propto r^{-4/3}$.

5.2. Wind Energy Balance

The kinetic calculation emphasizes the role of the ambipolar electric field in accelerating the wind. However, the large terminal wind velocity obtained with a Kappa distribution can also be understood by energy balance considerations involving the suprathermal electron heat flux in the corona, as suggested by *Olbert* [1981]. Let us calculate the electron parallel heat flux at any distance r. Neglecting the contributions of the terms due to bulk velocity, it can be approximated by the parallel kinetic energy flux of the escaping electrons

$$\begin{aligned} Q_{e\parallel}(r) &\approx \frac{m_e}{2}\int d^3v v^2 v_\parallel f_e(v) \quad (86)\\ &\approx \eta\,\frac{\pi m_e}{2}\int_{v_M}^{\infty} dv v^3 f_{e0}\left(\sqrt{v^2+V_e^2}\right)\left[v^2+V_e^2\right] \end{aligned}$$

With the change of variable $u = \sqrt{v^2+V_e^2}$ and using the expression (8) of the electron flux we find

$$Q_{e\parallel}(r) = \eta Q_{e\parallel}(r_0) - \frac{m_e V_e^2}{2}F_e(r) \quad (87)$$

We now approximate the wind energy balance by neglecting the electron and proton temperature terms, which is justified with a large terminal wind velocity, the small proton heat flux [*Lemaire and Scherer*, 1972], the small initial wind velocity (and the possible contribution from fluctuations and plasma waves). This gives the terminal wind velocity from

$$\frac{m_p V_{SW}^2}{2} \approx \frac{Q_{e\parallel}(r_0)}{F_e(r_0)} - \frac{Q_{e\parallel}(r)}{F_e(r)} - \Phi_g(r_0) \quad (88)$$

Substituting (87) with $V_e \approx V_0$ at large distances, this yields

$$\frac{m_p V_{SW}^2}{2} \approx \frac{m_e V_0^2}{2} - \Phi_g(r_0) \quad (89)$$

From the definitions (20) and (21) of V_0 and V_{p0}, this yields $V_{SW} \approx V_{p0}$, which is just the result found in section 4.1 with the same large wind velocity approximation. As expected, one can thus retrieve the terminal wind velocity from the energy balance, as produced by the electron heat flux at the exobase.

Note that, in particular, for either a Kappa distribution with $\kappa > 2$ and $U_0 \gg \kappa$ or a Maxwellian with $U_0 \gg 1$, (87) yields at any distance r

$$\frac{Q_{e\parallel}(r)}{F_e(r)} \approx \frac{m_e V_0^2}{2}\frac{\kappa-1}{\kappa-2} - \frac{m_e V_e^2}{2} \quad (90)$$

6. Summary and Final Remarks

We have found analytically a simple expression for the radial profile of the average electron temperature at large heliocentric distances in the solar wind by applying a kinetic model developed by *Lemaire and Scherer* [1971] to an arbitrary electron velocity distribution in the corona. The electron temperature does not follow a large-scale polytrope law, as is often assumed, but is instead the sum of a term varying as $r^{-4/3}$ plus a constant. The ratio of these terms is of order $(m_p/m_e)^{5/6}(r_0/r)^{4/3}$, so that since the exobase radius r_0 is a few solar radii, both terms are of the same order of magnitude near 1 AU. This result is weakly dependent on the particle velocity distributions in the corona. The relative contribution of the constant, which flattens the profile, tends to be larger in the fast wind coming from a polar coronal hole, where r_0 is expected to be smaller owing to the smaller density. This provides a natural explanation for the temperature profile generally observed and yields a flattening of the profile with increasing distance, in agreement with Helios observations [*Pilipp et al.*, 1990]. This analytical result is only valid at distances much larger than the exobase radius r_0; just above r_0, the temperature remains constant or increases, depending on whether the electron velocity distribution is Maxwellian or not (see section 3.1). All these results suggest that some care is needed when extrapolating to the corona empirical polytropic laws determined over a limited distance range.

This generic profile is not surprising. Indeed, the $r^{-4/3}$ temperature term, which comes from the electrons confined by the ambipolar electric potential, corresponds to an adiabatic behavior since their density varies as r^{-2}; this is not

surprising since they are isotropically distributed with zero heat flux. The temperature term which does not vary with distance comes from the parallel temperature of the escaping electrons; this behavior is not surprising since these electrons have negligible heat flux divergence (see (87)) and a small perpendicular temperature.

As expected, these analytical results are compatible with the anisotropic fluid momentum and energy balance equations for the whole electron population, but not with the isotropic ones. In particular, the isotropic momentum fluid equation, which is often used to estimate the heliospheric ambipolar potential, gives, in this case, an incorrect result.

Our calculation also gives explicit expressions for the ambipolar electric potential at large distances, which varies as $r^{-4/3}$, i.e., slightly more steeply than the Pannecoek-Rosseland potential, for the contribution of the escaping electrons to the total density, which is found to be a few percent, and for the terminal wind velocity. In particular, we show analytically that the terminal velocity increases when the electron velocity distribution at the exobase has more suprathermal electrons.

It must be noted that, for the sake of simplicity, we have neglected the solar rotation and assumed the magnetic field to be radial. This approximation may be acceptable to study the polar wind and also at smaller latitudes closer than 1 AU. For other regions the present results should be generalized to a spiral magnetic field [see *Chen et al.*, 1972]. It is also worth noting that the electrons trapped between the electrostatic and magnetic mirror reflection points have been assumed to be in quasi-equilibrium with those emerging from the exobase; at large distances these trapped electrons contribute much more than the ballistic ones to the moments of the distribution, so that the $r^{-4/3}$ temperature term is essentially due to them; relaxing this hypothesis would introduce an arbitrary coefficient for this term.

This model, which has the immense advantage of simplicity, has, however, some drawbacks. First, it is usual to identify (1) the confined electrons to the low-energy part of the observed electron distribution which is roughly Maxwellian and isotropic in its proper frame (the so-called "core"), which represents the bulk of the distribution, and (2) the escaping electrons to the high-energy part of the observed distribution which is highly anisotropic and asymmetric [*Mongomery et al.*, 1968; *Feldman et al.*, 1975] . However, in the exospheric description the confined electrons at large distances represent the low-energy part (with respect to the local heliospheric potential) of the exobase distribution translated in energy by a quantity roughly equal to the exobase potential; since the exobase temperature is of order 100 eV, the resulting distribution is very different from the core distribution observed near 1 AU, which is a quasi-Maxwellian of temperature of order 10 eV. Furthermore, the mean velocity of the core component is observed to be close to the solar wind velocity instead of zero, and the core temperature is observed to cool less steeply than adiabatically in the ecliptic [see, for example, *Sittler and Scudder,* 1980; *Pilipp et al.*, 1990] and also in the fast wind at high heliographic latitudes [*Issautier et al.*, 1998]. So, as expected, collisionless models do not predict correctly the electron velocity distribution nor separate contributions to the moments of arbitrary parts of the distribution, which are much more affected by collisions than the average total electron temperature.

Second, as noted in section 1, this model is not expected to predict correctly the proton temperature profile, and indeed, it does not. Third, although this model can give results in the range of observations for the shape of the average electron temperature radial profile and for the density and terminal velocity in both low- and high-speed winds and also for the electron temperature value in the low speed wind, a discrepancy still remains for the high-speed wind. Indeed, a Kappa distribution with a value of Kappa producing a large terminal velocity, i.e., $\kappa \leq 3$, results in an electron temperature at 1 AU more than twice as large as the typical values in the high-speed wind. This result, which can also be seen in the numerical results of *Maksimovic et al.* [1997a], is due to the contribution of the suprathermal electrons through velocity filtration [*Scudder*, 1992a, b]. Furthermore, it is easy to verify from the analytical formulae given in section 4 that changing the coronal thermal temperatures (within reasonable limits) does not solve this problem. Note also that the possible presence of non-Maxwellian protons at the exobase is not expected to solve this problem either. Indeed, increasing the number of suprathermal protons without changing the thermal temperature T_{p0} increases the proton flux, thereby requiring a smaller ambipolar potential to preserve the zero-current condition. As a consequence, a still smaller value of Kappa for the electron distribution is needed to achieve a large wind velocity, which, in turn, results in a still higher wind electron temperature.

A possible solution might be to start with distributions having an important anisotropy. A large velocity shift at a few solar radii has been suggested by recent observations in polar coronal holes [see for example *Grall et al.*, 1996], as well as possible temperature anisotropies. In this respect it is important to note that the ambipolar potential as well as the terminal velocity are mainly determined by the parallel temperatures at the exobase, whereas the perpendicular temperatures at the exobase mainly influence the average temperatures at large distances. Hence, for example, an increase of the proton perpendicular temperature at the exobase does not change our results.

Finally, it is important to note that the case studies of section 4.5 have only an illustrative value because of the simplifications made. A full model testing should involve accurate measurements in both the corona and the wind under well-defined conditions. Anyway, the above discussion illustrates the main deficiency of this class of exospheric solar wind models, which have the advantage of simplicity but neglect the fact that particles of different velocities have different exobase radii [see *Brandt and Cassinelli*, 1996; *Scudder and Olbert,* 1979] and circumvent the old-standing problem of calculating what happens in the transcollisional region below and near the exobase [see, for example, *Scudder and Olbert,* 1983; *Lie-Svendsen et al.*, 1997; *Pierrard and Lemaire,* 1998].

Appendix: Parameters D_q and B_q for a Kappa Distribution

The parameters D_q and B_q involved in the electron moments at large distances are obtained by substituting the Kappa distribution (53) into (28) and (29), respectively

$$D_q = \frac{2n_{e0}}{q+3}\frac{A_\kappa}{\left(\kappa w_e^2\right)^{3/2}}\left[1+\frac{U_0}{\kappa}\right]^{-(\kappa+1)} \quad \text{(A1)}$$

$$B_q = \frac{n_{e0}}{2}\frac{A_\kappa}{\left(\kappa w_e^2\right)^{3/2}}\left[1+\frac{V_0^2}{\kappa w_e^2}\right]^{-(\kappa+1)} \quad \text{(A2)}$$

$$\times \int_0^\infty dv v^q \left(v^2+V_0^2\right)\left[1+\frac{v^2}{V_0^2+\kappa w_e^2}\right]^{-(\kappa+1)}$$

With the identity $\beta_2(1) \equiv 1$ and the change of variable $x = 1/\left[1+v^2/\left(V_0^2+\kappa w_e^2\right)\right]$, β_2 being defined in (64), we deduce

$$B_0 = \frac{n_{e0}}{2}\left[1+\frac{U_0}{\kappa}\right]^{-\kappa-1/2}\left(U_0+1/2\right) \quad \text{(A3)}$$

$$B_2 = \frac{n_{e0}\kappa w_e^2}{2\left(2\kappa-3\right)}\left[1+\frac{U_0}{\kappa}\right]^{-\kappa+1/2}\left(U_0+3/2\right) \quad \text{(A4)}$$

Acknowledgments. We thank J. Lemaire, M. Velli, A. Mangeney, V. Pierrard, M. Moncuquet, F. Pantellini, M. Maksimovic, and J.L. Steinberg for stimulating discussions and useful comments on the manuscript.

The Editor thanks Oystein Lie-Svendsen and V. Pierrard for their assistance in evaluating this paper.

References

Brandt, J. C., and J. P. Cassinelli, Interplanetary gas, XI, An exospheric model of the solar wind, *Icarus, 5*, 47, 1966.

Chen, W. M., C. S. Lai, H. E. Lin, and W. C. Lin, Collisionless solar wind in the spiral magnetic field, *J. Geophys. Res., 77*, 1, 1972.

David, C., A. H. Gabriel, and F. Bely-Dubau, Temperature structure in coronal holes, Proceedings of 5th SOHO Workshop, *Eur. Space Agency Spec. Publ., SP-404*, 319, 1997.

Feldman, W. C., J. R. Asbridge, S. J. Bame, M. D. Mongomery, and S. P. Gary, Solar wind electrons, *J. Geophys. Res., 80*, 4181, 1975.

Fisher, R., and M. Guhathakurta, Physical properties of polar coronal rays and holes as observed with the Spartan 201-01 coronograph, *Astrophys. J., 447*, L139, 1995.

Grall, R.R., W.A. Coles, M.T. Klinglesmith, A.R. Breen, P.J.S. Williams, J. Markkanen, and R. Esser, Rapid acceleration of the polar solar wind, *Nature, 319*, 429, 1996.

Habbal, S.R., R. Esser, and M. Arndt, How reliable are coronal hole temperatures deduced from observations?, *Astrophys. J., 413*, 435, 1993.

Hernandez, R., S. Livi, and E. Marsch, On the He^{2+} to H^+ temperature ratio in slow solar wind, *J. Geophys. Res., 92*, 7723, 1987.

Issautier, K., N. Meyer-Vernet, M. Moncuquet, and S. Hoang, Pole to pole solar wind density from Ulysses radio measurements, *Sol. Phys., 172*, 335, 1997.

Issautier, K., N. Meyer-Vernet, M. Moncuquet, and S. Hoang, Solar wind radial and latitudinal structure: Electron density and core temperature from Ulysses thermal noise spectroscopy, *J. Geophys. Res., 103*, 1969, 1998.

Jockers, K., Solar wind models based on exospheric theory, *Astron. Astrophys., 6*, 219, 1970.

Ko, Y.-K., L. A. Kisk, G. Gloeckler, and J. Geiss, Limitations on suprathermal tails of electrons in the lower solar corona, *Geophys. Res. Lett., 23*, 2785, 1996.

Ko, Y.-K., L. A. Kisk, J. Geiss, G. Gloeckler, and M. Guhathakurta, An empirical study of the electron temperature and heavy ion velocities in the south polar coronal hole, *Sol. Phys., 171*, 345-361, 1997.

Kohl, J. L. , L. Strachan, and L. D. Gardner, Measurement of hydrogen velocity distributions in the extended corona, *Astrophys. J., 465*, L141, 1996.

Lemaire, J., and M. Scherer, Le champ électrique de polarisation dans l'exosphère ionique polaire, *C. R. Acad. Sci. Paris, 269B*, 666, 1969.

Lemaire, J., and M. Scherer, Kinetic models of the solar wind, *J. Geophys. Res., 76*, 7479, 1971.

Lemaire, J., and M. Scherer, Comportement asymptotique d'un modèle cinétique du vent solaire, *Bull. Cl. Sci. Acad. R. Belgium, 58*, 1112, 1972.

Lemaire, J., and M. Scherer, Kinetic models of the solar and polar winds, *Rev. Geophys., 11*, 427, 1973.

Lie-Svendsen, O, V. H. Hansteen, and E. Leer, Kinetic electrons in high-speed solar wind streams: formation of high-energy tails, *J. Geophys. Res., 102*, 4701, 1997.

Lin, R. P., Observations of the 3D distributions of thermal to near-relativistic electrons in the interplanetary medium by the wind spacecraft, in *Coronal Physics From Radio and Space Observations*, edited by G. Trottet, p. 93, Springer-Verlag, New-York, 1997.

Maksimovic, M., V. Pierrard, and J. Lemaire, A kinetic model of the solar wind with Kappa distribution functions in the corona, *Astron. Astrophys., 324*, 725, 1997a.

Maksimovic, M., V. Pierrard, and P. Riley, Ulysse electron distributions fitted with Kappa functions, *Geophys. Res. Lett., 24*, 1151, 1997b.

Marsch, E., W. G. Pilipp, K. M. Thieme, and H. Rosenbauer, Cooling of solar wind electrons inside 0.3 AU, *J. Geophys. Res., 94*, 6893, 1989.

Meyer-Vernet, N., M. Moncuquet, and S. Hoang, Temperature inversion in the Io plasma torus, *Icarus, 116*, 202, 1995.

Migdal, A. B., *Qualitative Methods in Quantum Theory*, Benjamin, White Plains, N.Y., 1977.

Mongomery, M. D., S. J. Bame, and A. J. Hundhausen, Solar wind electrons: Vela 4 measurements, *J. Geophys. Res., 73*, 4999, 1968.

Olbert, S., Inferences about the solar wind dynamics from observed distributions of electrons and ions, in *Plasma Astrophysics, Eur. Space Agency Spec. Publ., SP-161*, edited by T. D. Guyenne and G. Lévy, 1981.

Phillips, J.L., et al., Ulysses solar wind plasma observations from pole to pole, *Geophys. Res. Lett., 22*, 3301, 1995.

Pierrard, V., and J. Lemaire, Lorentzian ion exosphere model, *J. Geophys. Res., 101*, 7923, 1996.

Pierrard, V., and J. Lemaire, A collisional kinetic model of the polar wind, *J. Geophys. Res., 103*, 11,701 , 1998.

Pilipp, W. G., et al., Large scale variations of thermal electron parameters in the solar wind between 0.3 and 1 AU, *J. Geophys. Res., 95*, 6305, 1990.

Roberts, D. A., Generation of non-thermal electron distributions by turbulent waves near the Sun, *Geophys. Res. Lett., 25*, 607, 1998.

Schwenn, R., and E. Marsch, *Physics of the Inner Heliosphere*, vol. 2, Springer-Verlag, New-York, 1991.

Scudder, J. D., On the causes of temperature change in inhomogencous low-dcnsity astrophysical plasmas, *Astrophys. J., 398*, 299, 1992a.

Scudder, J. D., Why all stars should possess circumstellar temperature inversions, *Astrophys. J., 398*, 319, 1992b.

Scudder, J. D., and S. Olbert, A theory of local and global processes which affect solar wind electrons, 1, The origin of typical 1 AU velocity distribution functions - Steady state theory. *J. Geophys. Res.*, *84*, 2755, 1979.

Scudder, J. D., and S. Olbert, The collapse of the local, Spitzer-Härm formulation and a global-local generalization for heat flow in a inhomogeneous, fully ionized plasma, in *Solar Wind Five*, edited by M. Neugebauer, *NASA Conf. Publ., CP-2280,* 163, 1983.

Sittler, E. C., Jr., and J. D. Scudder, An empirical polytrope law for solar wind thermal electrons between 0.45 and 4.76 AU: Voyager 2 and Mariner 10, *J. Geophys. Res.*, *85*, 5131, 1980.

Spitzer, L., Jr., and R. Härm, Transport phenomena in completely ionized gas, *Phys. Rev.*, *89*, 977, 1953.

Tu, C.-Y., The damping of interplanetary Alfvénic fluctuations and the heating of the solar wind, *J. Geophys. Res.*, *93*, 7, 1988.

Withbroe, G.L., The temperature structure, mass, and energy flow in the corona and inner solar wind, *Astrophys. J.*, *325*, 442, 1988.

K. Issautier and N. Meyer-Vernet, Département de Recherche Spatiale, CNRS, Observatoire de Paris, 5 Place Jules Janssen, 92195 Meudon Cedex, France. (meyer@obspm.fr)

(Received January 20, 1998; revised July 17, 1998; accepted August 12, 1998.)